

# Follow-up observations of extremely metal-poor stars identified from SDSS. ★

D. S. Aguado<sup>1,2</sup>, C. Allende Prieto<sup>1,2</sup>, J. I. González Hernández<sup>1,2</sup>, R. Carrera<sup>1,2</sup>, R. Rebolo<sup>1,2,3</sup>, M. Shetrone<sup>4</sup>, D. L. Lambert<sup>4</sup>, E. Fernández-Alvar<sup>5</sup>

<sup>1</sup> Instituto de Astrofísica de Canarias, Vía Láctea, 38205 La Laguna, Tenerife, Spain

<sup>2</sup> Universidad de La Laguna, Departamento de Astrofísica, 38206 La Laguna, Tenerife, Spain

<sup>3</sup> Consejo Superior de Investigaciones Científicas, 28006 Madrid, Spain

<sup>4</sup> McDonald Observatory and Department of Astronomy, University of Texas, Austin, TX 78712, USA

<sup>5</sup> Instituto de Astronomía, Universidad Nacional Autónoma de México, AP 70-264, 04510 Ciudad de México, México

Received March 15, 2016; accepted June 1, 2016

## ABSTRACT

*Context.* The most metal-poor stars in the Milky Way witnessed the early phases of formation of the Galaxy, and have chemical compositions that are close to the pristine mixture from Big Bang nucleosynthesis, polluted by one or few supernovae.

*Aims.* Only two dozen stars with  $[\text{Fe}/\text{H}] < -4$  are known, and they show a wide range of abundance patterns. It is therefore important to enlarge this sample. We present the first results of an effort to identify new extremely metal-poor stars in the Milky Way halo.

*Methods.* Our targets have been selected from low-resolution spectra obtained as part of the Sloan Digital Sky Survey, and followed-up with medium resolution spectroscopy on the 4.2 m William Herschel Telescope and, in a few cases, at high resolution on the the 9.2 m Hobby-Eberly Telescope. Stellar parameters and the abundances of magnesium, calcium, iron, and strontium have been inferred from the spectra using classical model atmospheres. We have also derived carbon abundances from the G band.

*Results.* We find consistency between the metallicities estimated from SDSS and those from new data at the level of 0.3 dex. The analysis of medium resolution data obtained with ISIS on the WHT allow us to refine the metallicities and in some cases measure other elemental abundances. Our sample contains 11 new metal-poor stars with  $[\text{Fe}/\text{H}] < -3.0$ , one of them with an estimated metallicity of  $[\text{Fe}/\text{H}] \sim -4.0$ . We also discuss metallicity discrepancies of some stars in common with previous works in the literature. Only one of these stars is found to be C-enhanced at about  $[\text{C}/\text{Fe}] \sim +1$ , whereas the other metal-poor stars show C abundances at the level of  $[\text{C}/\text{Fe}] \sim +0.45$ .

*Conclusions.*

**Key words.** stars: Population II – stars: abundances – stars: Population III – Galaxy: abundances – Galaxy: formation – Galaxy: halo

## 1. Introduction

The oldest stars in the Milky Way belong to the halo and thick-disk populations (see, e.g. Reddy et al. (2006); Haywood et al. (2013)). The majority of the halo stars we can date seem to be older than about 10 Gyr, while stars in the thick disk can be as young as  $\sim 8$  Gyr (Allende Prieto et al. 2006). The metallicity distribution of the halo is broad (FWHM  $\sim 1.2$  dex), with an average metallicity of about  $[\text{Fe}/\text{H}] < -1.5$ , which has been recently found to shift to lower values at distances from the Galactic center of about 30 kpc (Carollo et al. 2008; Yong et al. 2012; Chen et al. 2014; Allende Prieto et al. 2014; Fernández-Alvar et al. 2015).

Compared to the disk population, the stellar halo has a very low density (about 1% of all stars in the solar neighborhood) but it becomes the dominant population at distances from the

plane larger than 4-5 kpc. Because these halo stars are far, they are difficult to observe. Deep spectroscopic surveys have been very helpful to study this population and, for example, over one million halo stars have spectroscopy from the Sloan Digital Sky Survey (SDSS, Yanny et al. 2009; Eisenstein et al. 2011).

The oldest halo stars are the most interesting, particularly those that formed in the first or second generation (Norris et al. 2013; Keller et al. 2014), and which must have primitive compositions, in particular very low metal abundances. Such objects are extremely rare as illustrates the fact that, despite substantial efforts, only 4 stars are known at  $[\text{Fe}/\text{H}] < -5$ . Theoretical calculations show that the lack of metals in the gas in the early universe prevents gas clouds from fragmenting effectively, and shifts the initial mass function to very high masses. The implication is that no low-mass stars were formed in the first generation (Bromm & Loeb 2003; Bonifacio et al. 2011, 2012). However, the minimum metallicity at which low-mass stars can form appears lower than suggested by theoretical predictions, and needs to be assessed empirically, as at least one unevolved F-type star, SDSS J10291+1729 (Caffau et al. 2011), not only shows  $[\text{Fe}/\text{H}] \approx -5$ ,

\* Based on observations obtained with the Hobby-Eberly Telescope, which is a joint project of the University of Texas at Austin, the Pennsylvania State University, Stanford University, Ludwig-Maximilians-Universität München, and Georg-August-Universität Göttingen.

but also low C and O abundances. Furthermore, it has been suggested that the C/Fe abundance ratios in extremely metal-poor stars exhibit a bimodal distribution (Caffau et al. 2014; Allende Prieto et al. 2015), which may be the result of two main types of supernovae coexisting in the early phases of evolution of our Galaxy.

The fraction of stars with large carbon enhancements increases significantly for low iron abundances (Cohen & Huang 2009; Bonifacio et al. 2015). These so-called Carbon enhanced metal-poor stars (CEMP) constitute about 30% of stars at  $[\text{Fe}/\text{H}] < -3.0$ , 40% at  $[\text{Fe}/\text{H}] < -3.5$ , and 75% at  $[\text{Fe}/\text{H}] < -4$ . Moreover, the four stars known at  $[\text{Fe}/\text{H}] < -5$  fall in this category. Currently, J10291+1729 sets the metallicity limit for the formation of low-mass stars, but is this an anomaly? are there many other stars with even lower iron abundances which are not enhanced in carbon or oxygen?

Solving these issues requires larger samples of extremely metal-poor stars (EMP). We present here a sample selected from SDSS spectra and observed on the William Herschel Telescope in La Palma, equipped with the medium resolution spectrograph ISIS. In Fig. 1 we show an example of the quality of the SDSS spectra and the ISIS spectra in the CaII H&K spectral region. Two of the stars have also been observed at higher resolution using HRS on the Hobby-Eberly Telescope at McDonald Observatory. Section 2 describes how the candidates were identified from SDSS spectra, §3 provides an account of the observations carried out and the data reduction, §4 details our spectroscopic analysis, and §7 summarizes our results and conclusions.

## 2. SDSS analysis and target selection

For a sample of more than a million objects with spectra consistent with zero redshift from the Sloan Extension for Galactic Understanding and Exploration (SEGUE, Yanny et al. 2009) and/or the Baryonic Oscillations Spectroscopic Survey (BOSS, Eisenstein et al. 2011; Dawson et al. 2013), we derive the stellar parameters: effective temperature  $T_{\text{eff}}$ , surface gravity  $\log g$ , and metallicity  $[\text{Fe}/\text{H}]$ <sup>1</sup>.

The SDSS optical spectra are from SDSS Data Release 9 (DR9, Ahn et al. 2012) for observations with the original SDSS spectrograph, and DR12 (Alam et al. 2015) for data obtained with the upgraded BOSS spectrographs (Smee et al. 2013). These optical spectra have modest signal-to-noise ratios and a resolving power of about 2,000. The spectral range 3850 – 9190 Å is matched to model spectra computed with classical model atmospheres.

We use an automatic pipeline based on FERRE<sup>2</sup> (Allende Prieto et al. 2006). The code divided the spectra in about 300/400~Å pieces, which are normalized to their mean fluxes, effectively removing low-frequency systematic errors in flux calibration and ISM extinction. The model spectra used in the analysis are treated exactly in the same fashion. The grid of synthetic spectra is the one described by Allende Prieto et al. (2014) but with the addition of the C-enhanced models. The carbon abundance is derived as a free parameter in the range  $-1.0 < [\text{C}/\text{Fe}] < +4.0$ , whereas the  $\alpha$ -element is set to  $[\alpha/\text{Fe}] = +0.4$ .

This analysis determines simultaneously the main three stellar parameters and the carbon abundances, assuming a microturbulence of  $2 \text{ km s}^{-1}$ . Table 1 provides the derived atmospheric

<sup>1</sup> We use the bracket notation for reporting chemical abundances:  $[a/b] = \log\left(\frac{N(a)}{N(b)}\right) - \log\left(\frac{N(a)}{N(b)}\right)_{\odot}$ , where  $N(x)$  represents number density of nuclei of the element  $x$ .

<sup>2</sup> FERRE is available from <http://hebe.as.utexas.edu/ferre>

parameters and carbon abundances, as well as the magnitudes, equatorial coordinates, and signal-to-noise ratio for each SDSS spectrum.

The effective temperatures and surface gravities derived from SDSS spectra were, in most cases, adopted for the subsequent analysis of the Spectrograph and Imaging System (ISIS) spectra. We consider our determination of effective temperatures very reliable. These are based on the fitting of the whole SDSS spectral range and of the local stellar continuum and Balmer lines, in particular (see Fig. 2). The estimated uncertainties have been discussed in detail by Allende Prieto et al. (2014), who compared the results from FERRE with those from the SEGUE Stellar Parameter Pipeline (SSPP, Lee et al. 2008a,b), finding a rms scatter between the two sets of values for halo stars of about  $\sigma_{T_{\text{eff}}} = 70 \text{ K}$ ,  $\sigma_{\log g} = 0.24$  and  $\sigma_{[\text{Fe}/\text{H}]} = 0.11$ . However, systematic errors for low gravity ( $\log g < 3$ ) stars have been detected from the comparison with the SSPP and the analysis of the globular cluster M13 (Allende Prieto et al. 2014). Taking those offsets into account the preferred gravity for J010505+461521 is  $\log g = 1.9$ , for J063055+255243 is  $\log g = 1.9$ , for J132250+012343 is  $\log g = 2.0$ , and for J165618+342523 is  $\log g = 2.1$ . Since our stars are on the low-metallicity edge of the distribution of halo stars, our uncertainties are likely somewhat higher than those inferred from these statistics. Fig. 3 shows DARMOUTH isochrones<sup>3</sup>, HB and AGB tracks compared to the stellar parameters derived with FERRE and its uncertainties. For this paper we adopt the following errors  $\sigma_{T_{\text{eff}}} = 150 \text{ K}$ ,  $\sigma_{\log g} = 0.3$  and  $\sigma_{[\text{Fe}/\text{H}]} = 0.2 \text{ dex}$  (see also Section 5.1).

We selected about a hundred EMP candidates from SDSS spectroscopy. All selected candidates have been classified in three priority levels, according to the quality of the spectrum, the goodness-of-fit for the Balmer lines, and the  $g$ -band magnitude. The signal-to-noise ratio varies across the sample, and we selected spectra with signal-to-noise ratios  $S/N > 15$ , with emphasis in targets at  $S/N > 30$ . The brightness distribution of the candidates makes it very difficult to find EMP candidates with high signal-to-noise ratios (exposure time is constant).

We included in our observations a few well-known metal poor stars, which are very useful to compare the performance of our methods with the results from the literature. More details are provided in the following section.

## 3. Observations and data reduction

### 3.1. Observations with ISIS on the 4.2m WHT

We obtained long-slit spectroscopy with ISIS (Jordan 1990), attached to the 4.2-m William Herschel Telescope (WHT), at the Roque de los Muchachos Observatory (La Palma) over the course of four observing runs; Run I: August 17-19 (3 nights), 2012; II: March 23-25 (3 nights), 2013; III: Dec 31 - Jan 2 (3 nights), 2015; IV: February 5-8 (4 nights), 2015. Twenty nine objects were observed in total. We used the R600B and R600R gratings, with the default dichroic, and a GG495 filter was used on the red arm. The observations were made with a one-arcsecond wide slit, the resolving power was  $R \sim 2400$  at 4500 Å in the blue arm, and  $R \sim 5400$  in the red arm. The instrument configuration was the standard ISIS R600B/R600R and the spectral ranges covered by the blue and red ISIS arms are 3500-5200 Å and 7420-9180 Å, respectively.

<sup>3</sup> The Dartmouth Stellar Evolution Program (DSEP) is available from [www.stellar.dartmouth.edu](http://www.stellar.dartmouth.edu)

**Table 1.** Coordinates and atmospheric parameters for the program stars based in the analysis of the SDSS spectra with the FERRE code. The FERRE internal uncertainties values in this table, discussed in section 2 are shown in brackets.

Star	$g$ mag	RA J2000 h ' ''	DEC J2000 ° ' ''	$T_{\text{eff}}$ K	$\log g$ $cm s^{-2}$	[Fe/H]	[C/Fe]	$\langle S/N \rangle^a$
SDSS J010505+461521	19.3	01:05:05.88	+46:15:21.60	5480	1.79	-3.86	-0.48	15
SDSS J014036+234458	15.8	01:40:36.22	+23:44:58.20	6092	4.77	-3.46	1.01	55
SDSS J021958-084955	16.4	02:19:58.25	-08:49:55.92	5705	3.97	-3.31	0.35	61
SDSS J040114-051259	18.6	04:01:14.71	-05:12:59.06	5854	4.98	-3.82	-0.79	39
SDSS J044655+113741	18.6	04:46:55.70	+11:37:41.16	5970	2.89	-3.30	0.67	23
SDSS J063055+255243	18.1	06:30:55.57	+25:52:43.72	5411	1.08	-3.61	0.78	42
SDSS J075818+653906	17.7	07:58:18.28	+65:39:06.95	6078	3.90	-3.25	0.71	25
SDSS J101600+172901	16.6	10:16:00.43	+17:29:01.32	5416	4.92	-3.40	0.01	49
SDSS J120441+120111	16.4	12:04:41.38	+12:01:11.64	5852	3.91	-3.55	-0.50	61
SDSS J123055+000547	14.8	12:30:55.25	+00:05:47.04	6199	4.18	-3.30	-0.25	51
SDSS J132250+012343	16.3	13:22:50.59	+01:23:43.08	5247	1.11	-3.58	0.78	62
SDSS J164234+443004	17.8	16:42:34.48	+44:30:04.96	6282	4.98	-4.61	0.55	32
SDSS J165618+342523	15.7	16:56:18.31	+34:25:23.16	5014	1.23	-3.08	-0.47	65
SDSS J183455+421328	19.1	18:34:55.03	+42:13:28.92	5367	4.92	-3.94	-0.45	17
SDSS J214633-003910	18.1	21:46:33.17	-00:39:10.08	6469	4.90	-4.85	0.57	18
SDSS J220646-092545	15.4	22:06:46.20	-09:25:45.84	4983	1.03	-3.07	0.45	53

<sup>a</sup> Signal-noise ratio have been calculated as average of the SDSS entire spectrum

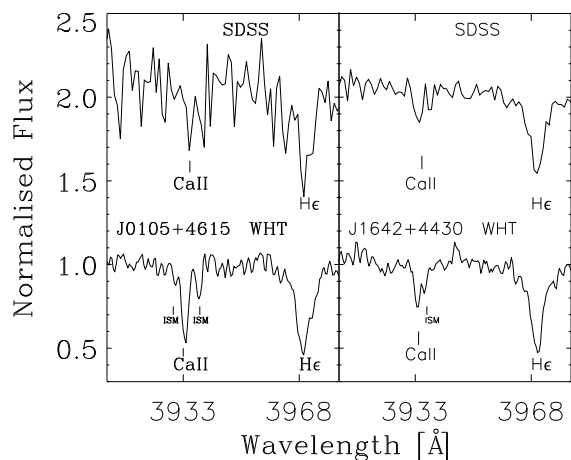


**Fig. 1.** Medium resolution SDSS spectra ( $R \sim 1800$ , top spectra) of two extremely metal-poor candidates, J0105+4615 (left panel) and J1642+4430 (right panel), together with ISIS spectra ( $R \sim 2400$ , bottom spectra) obtained at the 4.2m-WHT telescope. The Ca II K spectral lines from the star and the ISM are identified.

The information on the exposures obtained for each target is given in Table A.1. We lost about for nights of a total of 13 awarded for this project because of bad weather conditions. For purpose, we selected two targets identified from the HAMBURG-ESO survey, HE 1327-2326 (Frebel et al. 2005), one of the most metal-poor stars known, and HE 1523-0901 (Frebel et al. 2007), a strongly r-process-enhanced VMP in whose spectrum uranium has been detected. In addition, 2MASS

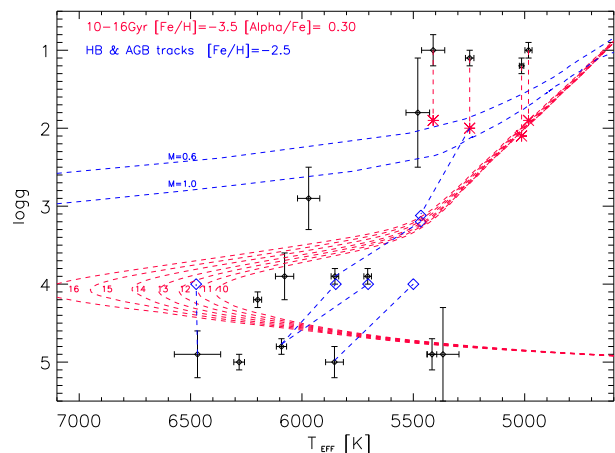


**Fig. 3.** DARMOUTH isochrones for  $[\text{Fe}/\text{H}] = -3.5$  and different ages from 16 to 10 Gyr (red dashed lines), blue dashed lines are HB and AGB theoretical tracks for  $[\text{Fe}/\text{H}] = -2.5$  for two different relative masses ( $M=0.6$  and  $M=1.0$ ). The black diamonds represent the stars of this work and its internal uncertainties derived from FERRE analysis. The red crosses are the four low-gravity objects explained in Section 2. The blue diamonds are bibliography values from Yong et al. (2013); Caffau et al. (2013); Placco et al. (2015) and discussed in Section 5.

J 2045-2842, a well-known ultra metal-poor star with moderately low effective temperature,  $T_{\text{eff}} \approx 4750$  K, was observed.

Data reduction included bias subtraction, flat-fielding, wavelength calibration (using CuNe + CuAr lamps), and com-

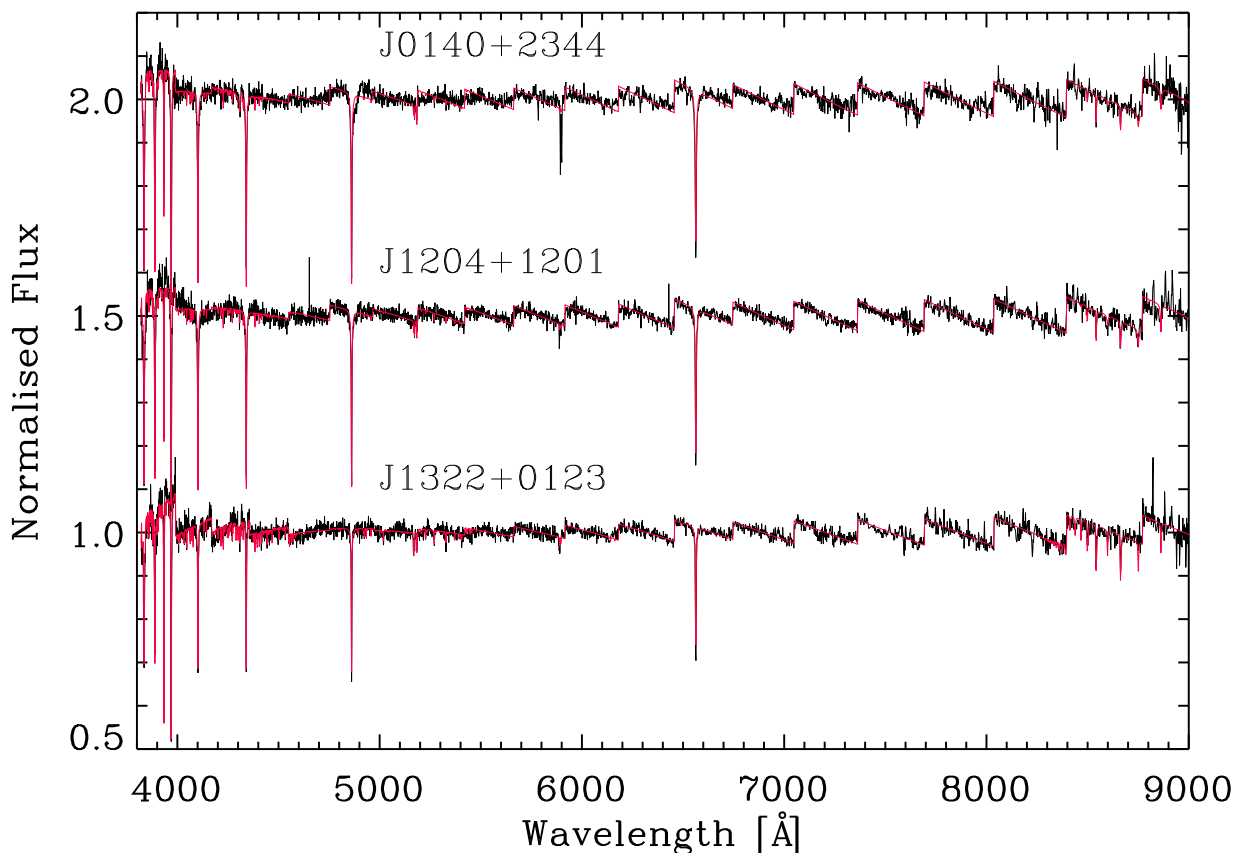


**Fig. 2.** SDSS spectra of J0140+2344, J1204+1201 and J1322+0123 (black line) analysed with. A reliable flux calibration allows to derive effective temperature using the slope of the continuum (red line).

bination of individual spectra, was performed using the *onespec* package in IRAF<sup>4</sup> (Tody 1993).

The ISIS spectra, with a resolution somewhat higher than those from SDSS, improve our chances of resolving potential contributions from the Interstellar Medium (ISM) to the absorption in the vicinity of the Ca II K line. In Fig. 1 we show several examples corresponding to candidates in which at least part of the ISM contribution can be identified in the ISIS spectrum while the SDSS low resolution do not allow us to do it. However, there are cases in which the ISM and stellar absorption cannot be resolved and our calcium abundances (and the corresponding iron abundances inferred from them) are, strictly speaking, upper limits. In Fig. 4 we depict the ISIS spectra together with synthetic spectra computed with the SYNTHE code (see Section 4.1) of all stars of our sample.

### 3.2. Observations with HRS on the 9.2m HET

The HRS (Tull et al. 1998) observations on HET (Ramsey et al. 1998) were obtained in service mode (Shetrone et al. 2007) over the period November 11, 2012 – March 22, 2013 at the McDonald Observatory (Texas). A total of 15.5 hours were allocated to this program, of which 2.5 and 8 hr were used for J0140+2344 and J0219–0849, respectively. The spectral range of these spectra spans 4000–5400 Å, with a gap between 4700 and 4800 Å. The resolving power was  $R \sim 15000$ , with 3.2 pixels per resolution element. The HRS configuration included two sky fibers, and  $2 \times 5$  binning on the CCDs. HRS/HET frames were processed with IRAF task *ccdproc* and *apflatten*. The extraction and wavelength-calibration were performed with the *echelle* package tasks within IRAF. The sky subtraction was performed with our own tools using the two HRS sky fibers. Finally the echelle orders of each spectrum were merged and normalized using the *norchelle* task developed by one of us<sup>5</sup>.

<sup>4</sup> IRAF is distributed by the National Optical Astronomy Observatory, which is operated by the Association of Universities for Research in Astronomy (AURA) under cooperative agreement with the National Science Foundation

<sup>5</sup> Available from Allende Prieto web page <http://www.as.utexas.edu/hebe/stools/>

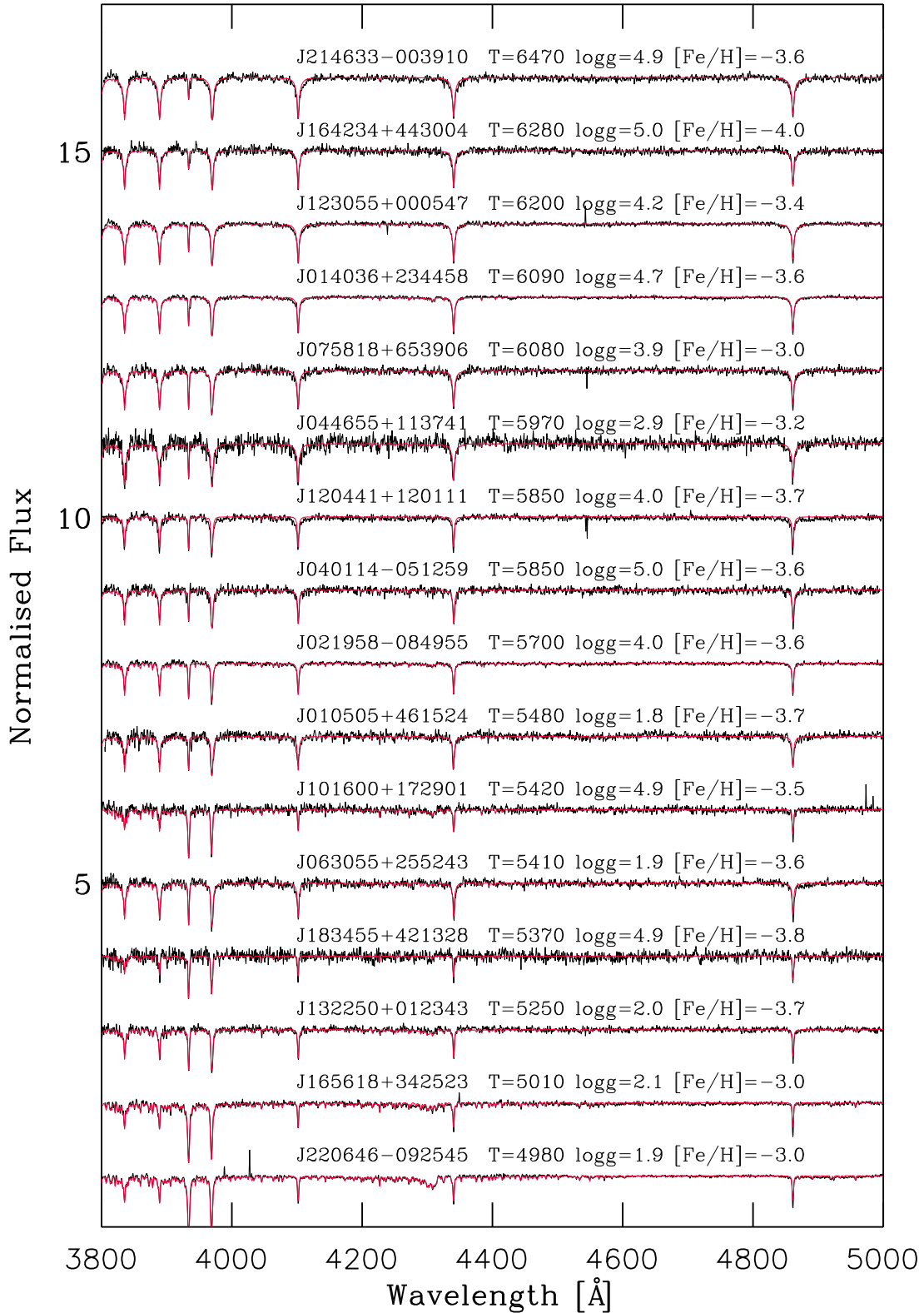


**Fig. 4.** The ISIS/WHT blue arm spectra (3800 Å-5000 Å) from the full sample (black line) and the best fit calculated with SYNTHE (red line). Over each spectrum the main stellar parameters are plotted.

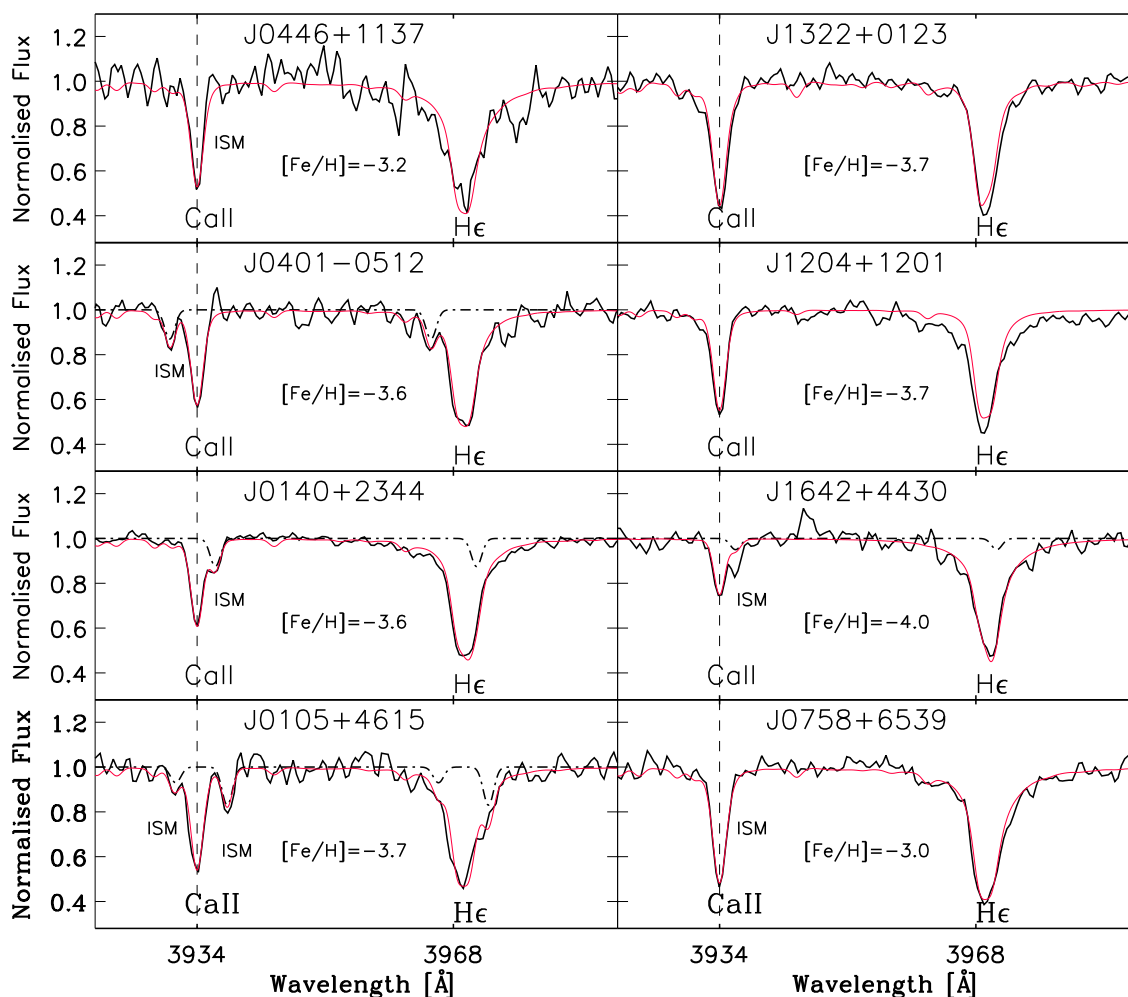


**Fig. 5.** ISIS spectra (solid black line) together with best fit synthetic spectra (solid red line) in the Ca II region for six different EMP, J0401–0512 (upper-left) with  $[\text{Fe}/\text{H}] = -3.6$ , J0140+2344 (middle-left) with  $[\text{Fe}/\text{H}] = -3.6$ , J0105+4615 (lower-left) with  $[\text{Fe}/\text{H}] = -3.7$ , J1642+4430 (upper-right) with  $[\text{Fe}/\text{H}] = -4.0$ , J0758+6539 (middle-right) with  $[\text{Fe}/\text{H}] = -3.0$ , J0446+1137 (lower-right) with  $[\text{Fe}/\text{H}] = -3.2$ , after the ISIS/WHT analysis. The ISM contribution in calcium K and H lines are added to the synthetic spectra (dashed-black line) calculated with SYNTHE.

## 4. Analysis

### 4.1. Analysis of ISIS spectra with MOOG and SYNTHE

Using the atmospheric parameters from the SDSS analysis, we calculate custom model atmospheres using ATLAS9 according to Mészáros et al. (2012). We measure the equivalent widths of the Ca II K line with the *splot* IRAF routine. Then, we derive calcium abundances analyzing the spectra with MOOG (Snedden 1973). These values are given in Table 2. Here we also assume  $[\alpha/\text{Fe}]=0.4$  and derive metallicities with  $[\text{Fe}/\text{H}]=[\text{Ca}/\text{H}]-[\alpha/\text{Fe}]$ . Then we check for consistency between the values obtained from the SDSS spectra and the calcium abundances from the equivalent-width method. The atomic data adopted for the lines analysed in this work are listed in Table 3. The solar abundance values adopted in this paper are  $A(\text{Mg})=7.53$ ,  $A(\text{Ca})=6.31$ ,  $A(\text{Sr})=2.92$  and  $A(\text{Fe})=7.45$  (Asplund et al. 2005).

The second and more thorough analysis of the ISIS spectra was performed using the code SYNTHE (Kurucz 2005; Sbor-

done 2005). We adopt the effective temperatures and surface gravities from SDSS spectra with the exception explained in section 2. Then manually optimize metallicity for each star. In nearly 85% of the cases the metallicity value inferred in this fashion is very close to the one from the analysis of the SDSS observations, suggesting that our SDSS results are fairly reliable. Table 2 summarizes the results from the SYNTHE analysis. The average offset of both metallicity determinations is  $[\text{Fe}/\text{H}]_{\text{SDSS}}-[\text{Fe}/\text{H}]_{\text{WHT}} = +0.21$  with a standard deviation of 0.31. Fig. 5 illustrates the agreement between model and ISIS blue-arm observations for eight of the stars in our sample in which there are several obvious ISM contributions to the absorption in the vicinity of the stellar Ca II K line. The top panel of Fig. 6 shows a well-known metal poor star, CS30336-0049 and one of our new identified metal-poor stars J1834–4213.

The equivalent-width method allows us to derive calcium abundances. The abundance uncertainty for this method is es-

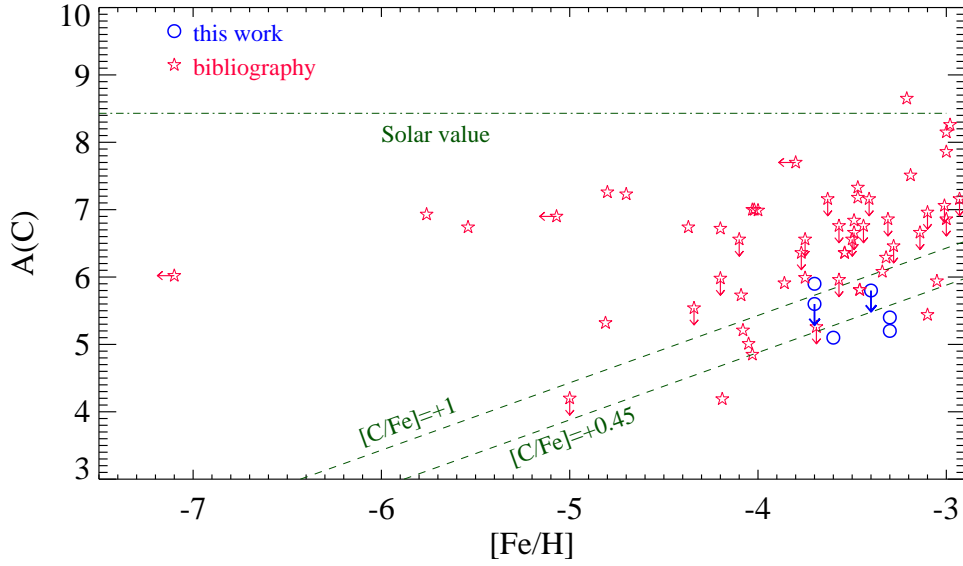
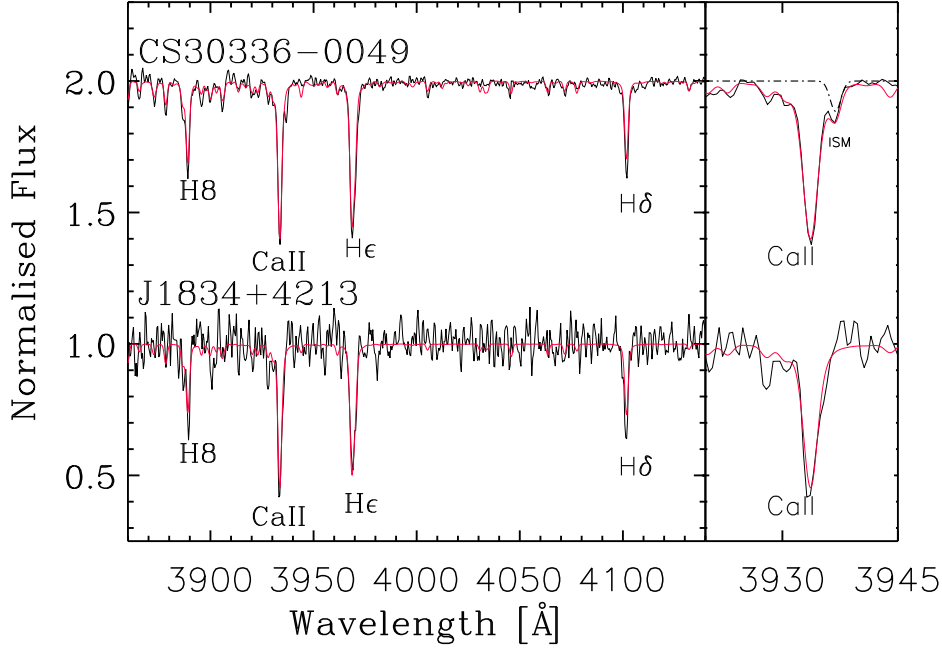


**Fig. 6.** *Upper panel:* ISIS spectra of CS30336-0049 (upper), a well-known metal-poor star with  $T_{\text{eff}} = 4750$ ,  $\log g = 1.19$  and  $[\text{Fe}/\text{H}] = -4.1$ , compared with SDSS J1834+4213 (lower), a new EMP with  $T_{\text{eff}} = 5370$ ,  $\log g = 4.9$  and  $[\text{Fe}/\text{H}] = -3.8$ . Carbon abundances versus metallicity of CEMP stars. Stars analysed in this work are represented by circles. The other stars (stars symbol) come from (Sivarani et al. 2006; Yong et al. 2013; Frebel et al. 2005, 2006; Caffau et al. 2014; Allende Prieto et al. 2015). The upper-dashed line represents the solar value  $A(\text{C})=8.43$  with very few CEMP stars over this value. A CEMP star defined as  $[\text{C}/\text{Fe}] > +1$  is plotted dashed line (Beers & Christlieb 2005b) and the mean carbon-to-iron ratio of turnoff extremely metal-poor stars, defined as  $[\text{C}/\text{Fe}] > +0.45$  (Bonifacio et al. 2009) is represented by dashed line.

**Table 2.** The stellar parameters and main results obtained from ISIS spectra.

Star	$T_{\text{eff}}$ [K]	$\log g$ [cm s <sup>-2</sup> ]	$\xi$ [km s <sup>-1</sup> ]	[Fe/H] <sub>SYNTHE</sub>	EW <sub>CaIK</sub> [Å]	A(Ca) <sub>MOOG</sub>	A(Ca) <sub>SYNTHE</sub>	A(C) <sub>SYNTHE</sub>
SDSS J010505+461521	5480	1.9	2.0	-3.7 ± 0.2	1.2 ± 0.1	3.1 ± 0.4	3.0 ± 0.2	-
SDSS J014036+234458	6090	4.7	2.0	-3.6 ± 0.2	0.7 ± 0.1	3.0 ± 0.4	3.2 ± 0.2	5.9 ± 0.4
SDSS J021958-084955	5700	4.0	2.0	-3.6 ± 0.2	1.3 ± 0.1	3.2 ± 0.4	3.2 ± 0.2	< 5.6
SDSS J040114-051259	5850	5.0	2.0	-3.6 ± 0.2	1.0 ± 0.1	3.0 ± 0.4	3.2 ± 0.2	-
SDSS J044655+113741	5970	2.9	2.0	-3.2 ± 0.2	0.9 ± 0.1	3.3 ± 0.4	3.6 ± 0.2	-
SDSS J063055+255243	5410	1.9	2.0	-3.6 ± 0.2	1.4 ± 0.1	3.0 ± 0.4	3.2 ± 0.2	-
SDSS J075818+653906	6080	3.9	2.0	-3.0 ± 0.2	1.2 ± 0.1	3.5 ± 0.4	3.8 ± 0.2	-
SDSS J101600+172901	5420	4.9	2.0	-3.5 ± 0.2	2.1 ± 0.1	3.1 ± 0.4	3.3 ± 0.2	5.1 ± 0.2
SDSS J120441+120111	5850	3.9	2.0	-3.7 ± 0.2	1.0 ± 0.1	2.9 ± 0.4	3.1 ± 0.2	-
SDSS J123055+000547	6200	4.2	2.0	-3.4 ± 0.2	0.9 ± 0.1	3.3 ± 0.4	3.4 ± 0.2	< 5.8
SDSS J132250+012343	5250	2.0	2.0	-3.7 ± 0.2	1.7 ± 0.1	3.2 ± 0.4	3.1 ± 0.2	-
SDSS J164234+443004	6280	5.0	2.0	-4.0 ± 0.2	0.5 ± 0.1	2.8 ± 0.4	2.8 ± 0.2	-
SDSS J165618+342523	5010	2.1	2.0	-3.3 ± 0.2	2.7 ± 0.1	3.3 ± 0.4	3.5 ± 0.2	5.2 ± 0.2
SDSS J183455+421328	5370	4.9	2.0	-3.8 ± 0.2	1.5 ± 0.1	2.8 ± 0.4	2.9 ± 0.2	-
SDSS J214633-003910	6470	4.9	2.0	-3.6 ± 0.2	0.7 ± 0.1	3.2 ± 0.4	3.2 ± 0.2	-
SDSS J220646-092545	4980	1.9	2.0	-3.0 ± 0.2	3.2 ± 0.1	3.5 ± 0.4	3.8 ± 0.2	5.4 ± 0.2

–The  $T_{\text{eff}}$  has been adopted from the FERRE results (see Table 1).

–The  $\log g$  has been adopted from the FERRE results in way shows in 2.

–The  $T_{\text{eff}}$  and  $\log g$  uncertainties are described in 2.

–The [Fe/H] has been derived from the [Ca/H] assuming  $[\alpha/\text{Fe}] = 0.4$ , following the expression  $[\text{Fe}/\text{H}] = [\text{Ca}/\text{H}] - [\alpha/\text{Fe}]$

–The [C/Fe] has been derived only in the cases the quality of the ISIS spectra is high enough.

**Table 3.** Atomic lines analysed in this work.

Element	$\lambda$ Å	E.P. eV	$\log gf$
Mg I	5167.321	2.709	-0.931
Mg I	5172.684	2.712	-0.450
Mg I	5183.604	2.717	-0.239
Ca I	4226.728	0.000	+0.265
Ca II	3933.663	0.000	+0.135
Fe I	5328.038	0.9146	-1.466
Fe II	5169.028	-0.87	+2.891
Sr II	4077.714	0.000	+0.148
Sr II	4215.552	0.00	-0.173

timated by the expression:

$$\sigma_{[\text{Ca}/\text{H}]}^2 = \left( \frac{\partial[\text{Ca}/\text{H}]}{\partial T_{\text{eff}}} \right)^2 \sigma_{T_{\text{eff}}}^2 + \left( \frac{\partial[\text{Ca}/\text{H}]}{\partial EW} \right)^2 \sigma_{EW}^2 + O(\log g) + O([\text{Fe}/\text{H}]) \quad (1)$$

neglecting the terms depending on  $\log g$  and [Fe/H] We estimate an uncertainty of 0.1 Å in the EW<sub>CaIK</sub> values measured with *splot*. The uncertainties in  $T_{\text{eff}}$  are given in Section 2. Following this procedure we obtain  $0.3 \text{ dex} < \sigma_{[\text{Ca}/\text{H}]} < 0.4 \text{ dex}$  for the Ca abundances derived from equivalent width measurements of the Ca II K line. In Table 2 we have adopted the more conservative  $\sigma_{[\text{Ca}/\text{H}]} = 0.4$ .

However, we obtain more precise Ca abundances using SYNTHE, which allows us to fit the entire spectrum in more detail. In practice we compare the observations with models computed for an array of abundances in steps of 0.05 dex. By varying the values of effective temperatures and surface gravities taking into account the uncertainties previously discussed for the

SDSS analysis, we derive uncertainties of 0.2 dex in the SYNTHE calcium abundances. The final metallicity uncertainties in Section 2 are derived from  $[\text{Fe}/\text{H}] = [\text{Ca}/\text{H}] - [\alpha/\text{Fe}]$ , assuming  $[\alpha/\text{Fe}] = 0.4$

#### 4.2. Carbon abundance

As discussed in the Introduction, CEMP stars are specially frequent among the most metal-poor stars. It has been proposed that there is a bimodality of carbon abundances in CEMP stars in the  $[\text{Fe}/\text{H}] < -3.5$  regime (Spite et al. 2013; Bonifacio et al. 2015; Allende Prieto et al. 2015; Hansen et al. 2015a).

A population of stars shows higher carbon abundances,  $A(\text{C}) \sim 8.25$  than the other,  $A(\text{C}) \sim 6.5$ . Some CEMP stars exhibit high abundances of slow neutron-capture elements and are defined by  $[\text{Ba}/\text{Fe}] > +1.0$  (CEMP-s stars). On the other hand, CEMP-no stars do not show such high abundances of s-process elements and  $[\text{Ba}/\text{Fe}] < +0.0$  (Beers & Christlieb 2005a).

Using SDSS spectra we are able to measure the carbon abundance only in few cases, when the G band is clean enough and the S/N ratio is high enough.

For the stars in our sample, we can use the G band at  $\sim 4300 \text{ Å}$  to derive carbon abundances (Lambert & Sawyer 1984) thanks to the higher ISIS spectra resolving power and, in several cases, higher S/N. We manually fit the spectra with SYNTHE, the same process followed for deriving calcium abundances. Our results are included in Table 2. Fig. 7 shows all the cases for which we detect the G band, but only upper limits are provided in some cases due to the weakness of the G band in those stars. The lower effective temperature the easier the carbon detection.

In the bottom panel of Fig. 6 we display the [C/Fe] ratios versus the metallicity [Fe/H] of the stars in our sample, together with the stars from the literature. Three of stars analysed in this work, J101600+172901, J165618+342523, J220646-092545, do not give extra information about the nature of CEMP because

**Table 4.** J0140+2344 atmospheric parameters.

Author	$T_{\text{eff}}$	[Fe/H]	$\log g$	[C/Fe]
Yong et al. (2013)	5703	-4.0	4.68	+1.13
Caffau et al. (2013)	5848	-3.83	4.0	$\leq 1.4$
This work	6090	-3.6	4.77	+1.07

all are at about the level of  $[C/Fe] \sim +0.45$ , and are “normal” metal-poor turn-off stars (Behara et al. 2010; Masseron et al. 2010; Cohen et al. 2013). In the case of J021958–084955 and J123055+000547 we are only able to give an upper limit to the carbon abundances. Probably this two stars are also “normal” metal-poor turnoff stars. Finally J014036+234458 is the only star with  $[C/Fe] > +1.0$  and the most metal-poor star of this sub-sample, according to the statistics mentioned in Section 1.

The ISIS medium-resolution data are only in few cases able to detect the G band absorption. We have estimated the uncertainties from the difference between the best fit model and visually identified upper limits. This was only possible in four cases, given in Table 2.

## 5. Comparison with previous work

Five of our targets have been observed and analyzed in recent independent studies. As explained in §2 and §4.1, we derive the calcium abundance from the resonance Ca II K line and assume  $[\alpha/Fe] = +0.4$  to derive a metallicity. Below we compare our results with those in the literature.

### 5.1. SDSS J014036+234458

The analysis of the SDSS and ISIS spectra of J0140+2344 leads to  $T_{\text{eff}} = 6090 \pm 200$  K,  $\log g = 4.7 \pm 0.3$  and  $[Fe/H] = -3.6 \pm 0.2$ . The continuum slope fit suggests (See Fig. 2 the general uncertainty adopted in 2 have to increase to 200 K. However Yong et al. (2013) uses a high resolution spectrum obtained with HIRES at the Keck-I telescope to derive  $T_{\text{eff}} = 5703 \pm 85$  K and  $[Fe/H] \approx -4.0$ . On the other hand, Caffau et al. (2013) using X-SHOOTER at VLT spectra derive  $T_{\text{eff}} = 5848$  K, and  $[Fe/H] = -3.83$  assuming  $\log g = 4.0$ . The differences among the three  $[Fe/H]$  values are most likely related to the different adopted temperatures. In Fig. 8 we display the ISIS spectrum of this star, together with three synthetic spectra. The best fitting of the Balmer lines appears to correspond to our  $T_{\text{eff}}$  value. While the SYNTH code use Ali & Griem (1966) theory for self-broadening of Balmer lines in order to derive effective temperature Yong et al. (2013); Caffau et al. (2013) use the Barklem et al. (2000a,b) theory. In principle, Sbordone et al. (2010) showed about +350 K disagreement at the level of 5800 K and +200 K at 6100 K, between effective temperatures derived from  $H\alpha$ . Using both theories, providing the the Ali & Griem (1966) theory hotter temperature scale. However we note here that our  $T_{\text{eff}}$  has been derived with FERRE, using a grid of model synthetic spectra computed with the ASSET code (Koesterke et al. 2008), which also uses the Barklem theory for Balmer lines but also the slope of the continuum. In Fig. 8 we plot synthetic spectra for different set of parameters using ASSET. Our C abundance,  $A(C) = 5.9 \pm 0.4$ , which is compatible with the reference value from the literature,  $A(C) = 5.56 \pm 0.04$ , was derived assuming the star is a dwarf (Yong et al. 2013). Moreover, Caffau et al. (2013) only give an upper limit for carbon abundance of  $A(C) \leq 6.0$ .

### 5.2. SDSS J040114–051259

The metallicity derived by Caffau et al. (2013),  $[Fe/H] = -3.62$ , is the same as that derived in this work. Nevertheless, the derived effective temperature,  $T_{\text{eff}} = 5500$  K, is significantly different from our value,  $T_{\text{eff}} = 5850$  K. In Fig. 8 we depict the synthetic spectra with both sets of parameters and the best-fit calcium abundance. The synthetic spectrum, even though computed with ASSET, using our stellar parameters seems to well reproduce better the ISIS spectrum of this star (see Fig 8).

### 5.3. SDSS J120441+120111

The main stellar parameters derived from the analysis of SDSS spectra by Placco et al. (2015),  $T_{\text{eff}} = 5894$  K,  $\log g = 2.66$ ,  $[Fe/H] = -3.41$  are in fair agreement with our own results:  $T_{\text{eff}} = 5850$  K,  $\log g = 3.9$ , and  $[Fe/H] = -3.7$ . However the authors proposed a different set of parameters based on a high-resolution spectrum obtained using MIKE spectrograph at the 6.5m Magellan telescope,  $T_{\text{eff}} = 5467$  K,  $\log g = 3.20$  and  $[Fe/H] = -4.34$ . This metallicity difference of about 0.6 dex is easily explained by the 400 K difference.

Placco et al. (2015) provide the equivalent widths for 22 iron lines, the Ca K line and the Ca I transition at 4226 Å. Assuming our atmospheric parameters we have derived the following values using *Abfind* routine with MOOG:  $[Fe I/H] = -3.9$ ,  $[Ca I/H] = -3.7$  and  $[Ca II/H] = -3.8$  while, according to our SYNTH analysis, we derive  $[Ca II/H] = -3.3$  for the resonance calcium K line. As described in Section 2, our  $T_{\text{eff}}$  determination is based on simultaneous fitting of the stellar continuum and Balmer lines and therefore we consider it more reliable than the high resolution analysis which is based on excitation equilibria of Fe I lines and after corrected procedure explained in Placco et al. (2015), and references therein.

### 5.4. SDSS J132250+012343

Following a similar process as in the case of J1204+1201, Placco et al. (2015) derived  $T_{\text{eff}} = 5466$  K,  $\log g = 3.12$ , and  $[Fe/H] = -3.32$  from its SDSS spectrum. This is somewhat different from our results based on the same data:  $T_{\text{eff}} = 5250$  K,  $\log g = 2.0$ ,  $[Fe/H] = -3.7$ . The same authors, using a high resolution spectrum, derived a slightly different set of parameters,  $T_{\text{eff}} = 5008$  K,  $\log g = 1.95$ ,  $[Fe/H] = -3.64$  which are compatible with our own results. The equivalent widths measured by Placco et al. (2015) with our stellar parameters lead to  $[Ca I/H] = -3.2$  and  $[Fe I/H] = -3.3$ .

### 5.5. SDSS J214633–003910

The SDSS spectrum of J2146-0039 has a poor quality in terms of low signal-to-noise ratio. However, our pipeline derives  $T_{\text{eff}} = 6470$  K, in good agreement with the value reported by Caffau et al. (2013), who find  $T_{\text{eff}} = 6475$  K. In addition, both analyses suggest that J2146-0039 is a dwarf.

The metallicity proposed by Caffau et al. (2013), derived using a high-resolution spectrum, is  $[Fe/H] = -3.14$ , while our preferred value is 0.4 dex lower,  $[Fe/H] = -3.6$ . We are able to resolve a significant contribution to the observed feature from interstellar calcium at 3933 Å. A more detailed analysis in order to resolve this discrepancy is needed.

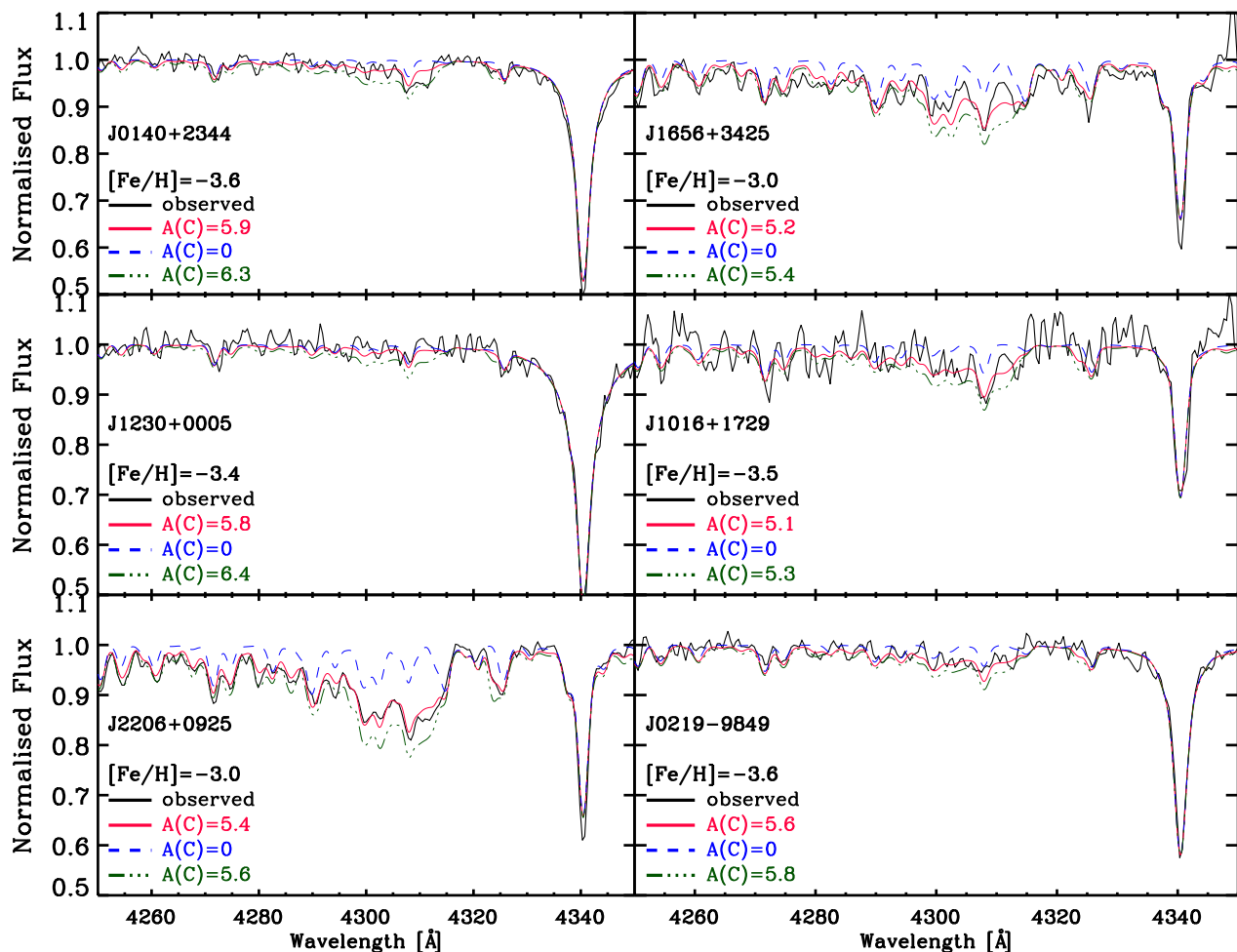


**Fig. 7.** Six stars reported in this work. The black line shows the observed spectrum, the red one is the best fitting model calculated with SYNTHE, the blue-dashed curve corresponds to the case the stars are not enhanced in carbon relative to solar C/Fe abundance ratios, and the green dotted line corresponds to upper limits. In four cases we are able to give a value for carbon abundance J0140+2344, J1016+1729, J1656+3425 and J2206+0925 and upper limits are given for the other two stars, J0219-9849, J1230+0005.

## 6. Analysis of HET spectra with SYNTHE

High-resolution ( $R \sim 15,000$ ) spectroscopic observations of the stars J0140+2344 and J0219-0849 were carried out in order to determine the abundances of Fe, Mg, and Sr in these stars. The effective temperatures and surface gravities from our analysis of their SDSS spectra were adopted. For both stars, the signal-to-noise of the spectra from the HRS red chip (4800 Å- 5400 Å) is higher than those from the blue one (4000 Å- 4700 Å), with only a few elements that could be analyzed. We find that our results from HRS/HET observations are compatible with those from ISIS. We include the derived chemical abundances in Table 5.

### 6.1. J014036+234458

Yong et al. (2013) provide complete information about the chemical abundances derived using the stellar parameters discussed in §5.1. According to our results, the discussion in this section assumes J0140+2344 is a dwarf star ( $\log g = 4.7$ ). The only Fe I line we are able to measure at 4328 Å gives us the iron abundance  $A(\text{Fe I})=3.8$  (see table 5) or  $[\text{Fe}/\text{H}]=-3.6$  in perfect agreement with the metallicity derived in Section 4.1. We propose a magnesium abundance  $A(\text{Mg I})= 4.4 \pm 0.2$  while Yong et al. (2013) derived  $3.86 \pm 0.06$ . There is a gap of about 0.5 dex between these two values, which could be explained by the difference effective temperatures adopted in the two analyses. For Ca I we can only set an upper limit  $A(\text{Ca I}) < 3.5$ , while Yong et al. (2013) determined  $A(\text{Ca}) = 2.53 \pm 0.06$ . A similar situation is found for Sr, with an abundance of  $A(\text{Sr II})= 0.01 \pm 0.06$  obtained by Yong

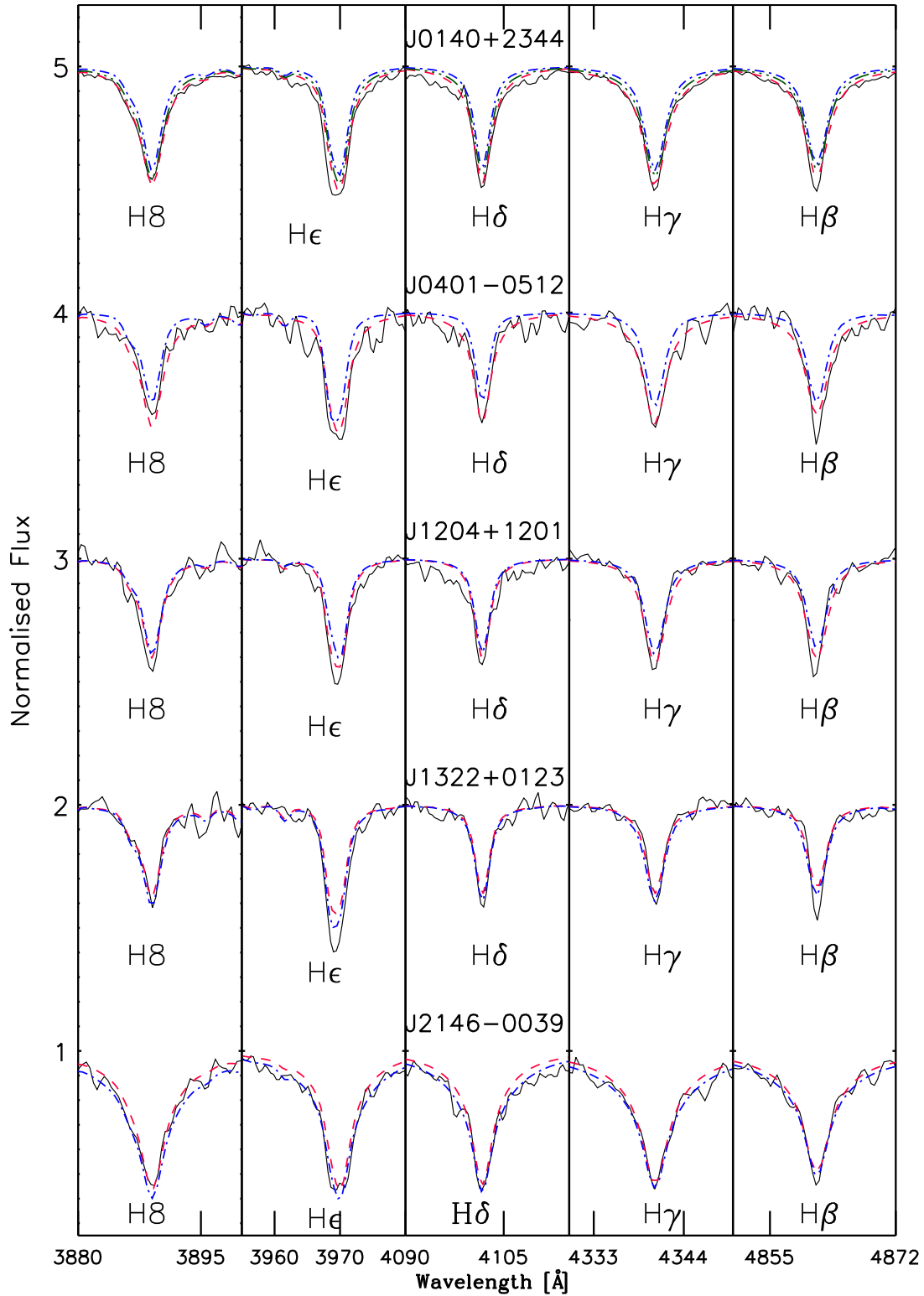


**Fig. 8.** ISIS spectrum of the stars J0140+2344, J0401-0512, J1204+1201, J1322+0123 and J2146-0039 (black solid lines) and best fit obtained in this work (red dashed line) performed with ASSET with the set of parameters  $\langle T_{\text{eff}}, \log g, [\text{Fe}/\text{H}] \rangle$ , [6090, 4.7, -3.6], [5850, 5.0, -3.6], [5850, 3.9, -3.7], [5250, 2.0, -3.7], [6470, 4.9, -3.6], respectively. Two additional synthetic spectra are depicted for J0140+2344: one (green triple-dotted-dashed-line) using  $T_{\text{eff}} = 5848$  K,  $\log g = 4.0$ ,  $[\text{Fe}/\text{H}] = -3.83$  (Caffau et al. 2013) and other spectrum (blue triple-dotted-dashed-line)  $T_{\text{eff}} = 5703$  K,  $\log g = 4.0$ ,  $[\text{Fe}/\text{H}] = -4.00$  (Yong et al. 2013). One spectrum for the other objects (blue dotted-dashed line) with values: [5500, 4.0, -3.6] for J0401-0512 (Caffau et al. 2013), [5467, 3.2, -4.34] for J1204+1201 (Placco et al. 2015), [5466, 3.12, -3.32] for J1322+0123 (Placco et al. 2015) and [6475, 4.0, -3.14] for J2146-0039 (Caffau et al. 2013).

**Table 5.** HET abundances.

Object	A(Mg I)	A(Ca I)	A(Sr II)	A(Fe I)	A(Fe II)
J0140+2344	$4.4 \pm 0.2$	$< 3.5$	$< 0.5$	$3.8 \pm 0.2$	$< 3.3$
J0219-0849	$4.2 \pm 0.2$	$< 3.2$	$< 0.7$	$4.0 \pm 0.2$	$3.9 \pm 0.2$

et al. (2013), compared to our upper limit of  $A(\text{Sr II}) < 0.5$ . It seems the 0.3 dex gap in metallicity and various elemental abundances are closely linked to the difference of 300 K in effective temperature.

## 6.2. J021958–084955

The red part of the spectrum allows us to measure the magnesium abundance and a single iron line (5325 Å). Upper limits for other chemical abundances are given in Table 5. In Fig. 9 we depict the observed HRS spectra of the stars J0219-0849 and J0140+2344, together with synthetic spectra for our best-fitting parameters. The uncertainties involved in high resolution spectroscopic analysis have been discussed by Allende Prieto et al. (2008). Our error bars are included in Table 5, where only upper limits are given for some elements.

## 7. Discussion and conclusions

We carry out a combined analysis of SDSS and ISIS/WHT spectroscopy to identify several extremely low metallicity stars. The candidates are selected after analysis of the SDSS data, and followed up with high quality ISIS/WHT and HRS/HET observations. From the comparison of the metallicities we inferred from SDSS spectra with those from our analysis of ISIS/WHT data, HRS/HET data, and the literature when available, we conclude that our selection based on SDSS spectra is highly reliable. In Fig. 8 we plot the carbon abundance for several CEMPS with  $[\text{Fe}/\text{H}] < -4.0$ , and several more in the  $[\text{Fe}/\text{H}] < -3.0$  regime. Two of our objects, J 1656+3425 and J 2206-0925, are giant stars and it is possible that their carbon abundance can be somewhat affected by mixing in deep layers (Spite et al. 2005).

The two main sub-classes of the CEMP stars (the CEMP-no and CEMP-s stars) are discussed in Section 4.2. Hansen et al. (2015a) suggest that CEMP-s stars are generally the product of mass transfer from a asymptotic giant-branch (AGB) star companion. This mass transfer could be the origin of the carbon enrichment, which would explain why most of the CEMP-s stars exhibit very high carbon abundances (Bonifacio et al. 2015). Over 90% of the stars located in the band with very high carbon enhancements are CEMP-s or CEMP-rs. The source of the s-process elements in CEMP-s stars are not well explained yet. Nevertheless, the carbon in CEMP-no stars was provided by their natal molecular clouds (Starkenbug et al. 2014). In fact, CEMP-no stars could be part of binary systems, but their enhanced carbon does not have an origin in a mass-transfer process. The aforementioned authors refer to these objects as bona-fide fossil records because the abundances in these objects reflect those in the interstellar medium where they were formed (Bonifacio et al. 2015; Hansen et al. 2015b).

Several questions related to the formation and composition of EMP, UMP and HMPs still remain unresolved. The fact that SDSS J102915+172927 (Caffau et al. 2011) is the only known UMP unevolved star with  $[\text{C}/\text{Fe}] < +1$  is not yet understood. On the other hand, faint supernova models (see e.g. Tominaga et al. (2014)) or models of *spinstars*, massive rotating metal-poor stars, see e.g. Maeder et al. (2015), seem to explain the main fea-

tures of the abundance patterns of CEMP, CEMP-no stars, but surely still more identification of stars at extremely low metallicities are need to better understand the formation of these stars in the early Universe. This paper describes our observational program. Additional observations are taking place and will be used to try to answer some of the previous questions.

*Acknowledgements.* DA acknowledges the Spanish Ministry of Economy and Competitiveness (MINECO) for the financial support received in the form of a Severo-Ochoa PhD fellowship, within the Severo-Ochoa International PhD Program. DA, CAP, JIGH, RR also acknowledge the Spanish ministry project MINECO AYA2014-56359-P. JIGH acknowledges financial support from the Spanish Ministry of Economy and Competitiveness (MINECO) under the 2013 Ramón y Cajal program MINECO RYC-2013-14875. DLL acknowledges the support of the Robert A. Welch Foundation through grant F-634. EFA acknowledges support from DGAPA-UNAM postdoctoral fellowships. This paper is based on observations made with the William Herschel Telescope, operated by the Isaac Newton Group at the Observatorio del Roque de los Muchachos, La Palma, Spain, of the Instituto de Astrofísica de Canarias. We thank ING staff members for very efficiently during the four observing runs in visitor mode. The Hobby-Eberly Telescope (HET) is a joint project of the University of Texas at Austin, the Pennsylvania State University, Stanford University, Ludwig-Maximilians-Universität München, and Georg-August-Universität Göttingen. The HET is named in honor of its principal benefactors, William P. Hobby and Robert E. Eberly.

## References

- Ahn, C. P., Alexandrov, R., Allende Prieto, C., et al. 2012, *ApJS*, 203, 21  
 Alam, S., Albareti, F. D., Allende Prieto, C., et al. 2015, *ApJS*, 219, 12  
 Ali, A. W. & Griem, H. R. 1966, *Physics Letters A*, 366, 144  
 Allende Prieto, C., Beers, T. C., Wilhelm, R., et al. 2006, *ApJ*, 636, 804  
 Allende Prieto, C., Fernández-Alvar, E., Aguado, D. S., et al. 2015, *A&A*, 579, A98  
 Allende Prieto, C., Fernández-Alvar, E., Schlesinger, K. J., et al. 2014, *A&A*, 568, A7  
 Allende Prieto, C., Sivarani, T., Beers, T. C., et al. 2008, *AJ*, 136, 2070  
 Asplund, M., Grevesse, N., & Sauval, A. J. 2005, in *Astronomical Society of the Pacific Conference Series*, Vol. 336, *Cosmic Abundances as Records of Stellar Evolution and Nucleosynthesis*, ed. T. G. Barnes, III & F. N. Bash, 25  
 Barklem, P. S., Piskunov, N., & O’Mara, B. J. 2000a, *A&AS*, 142, 467  
 Barklem, P. S., Piskunov, N., & O’Mara, B. J. 2000b, *A&A*, 355, L5  
 Beers, T. C. & Christlieb, N. 2005a, *ARA&A*, 43, 531  
 Beers, T. C. & Christlieb, N. 2005b, *Highlights of Astronomy*, 13, 579  
 Behara, N. T., Bonifacio, P., Ludwig, H.-G., et al. 2010, *A&A*, 513, A72  
 Bonifacio, P., Caffau, E., François, P., et al. 2011, *Astronomische Nachrichten*, 332, 251  
 Bonifacio, P., Caffau, E., Spite, M., et al. 2015, *A&A*, 579, A28  
 Bonifacio, P., Sbordone, L., Caffau, E., et al. 2012, *A&A*, 542, A87  
 Bonifacio, P., Spite, M., Cayrel, R., et al. 2009, *A&A*, 501, 519  
 Bromm, V. & Loeb, A. 2003, *Nature*, 425, 812  
 Caffau, E., Bonifacio, P., François, P., et al. 2011, *Nature*, 477, 67  
 Caffau, E., Bonifacio, P., Sbordone, L., et al. 2013, *A&A*, 560, A71  
 Caffau, E., Sbordone, L., Bonifacio, P., et al. 2014, *Mem. Soc. Astron. Italiana*, 85, 222  
 Carollo, D., Beers, T. C., Lee, Y. S., et al. 2008, *Nature*, 451, 216  
 Chen, Y. Q., Zhao, G., Carrell, K., et al. 2014, *ApJ*, 795, 52  
 Cohen, J. G., Christlieb, N., Thompson, I., et al. 2013, *ApJ*, 778, 56  
 Cohen, J. G. & Huang, W. 2009, *ApJ*, 701, 1053  
 Dawson, K. S., Schlegel, D. J., Ahn, C. P., et al. 2013, *AJ*, 145, 10  
 Eisenstein, D. J., Weinberg, D. H., Agol, E., et al. 2011, *AJ*, 142, 72  
 Fernández-Alvar, E., Allende Prieto, C., Schlesinger, K. J., et al. 2015, *A&A*, 577, A81  
 Frebel, A., Aoki, W., Christlieb, N., et al. 2005, *Nature*, 434, 871  
 Frebel, A., Christlieb, N., Norris, J. E., et al. 2006, *ApJ*, 652, 1585  
 Frebel, A., Christlieb, N., Norris, J. E., et al. 2007, *ApJ*, 660, L117  
 Hansen, C. J., Nordstroem, B., Hansen, T. T., et al. 2015a, *ArXiv e-prints* [arXiv:1511.07812]  
 Hansen, T. T., Andersen, J., Nordström, B., et al. 2015b, *ArXiv e-prints* [arXiv:1511.08197]  
 Haywood, M., Di Matteo, P., Lehnert, M. D., Katz, D., & Gómez, A. 2013, *A&A*, 560, A109  
 Jorden, P. R. 1990, in *Society of Photo-Optical Instrumentation Engineers (SPIE) Conference Series*, Vol. 1235, *Instrumentation in Astronomy VII*, ed. D. L. Crawford, 790–798  
 Keller, S. C., Bessell, M. S., Frebel, A., et al. 2014, *Nature*, 506, 463  
 Koesterke, L., Allende Prieto, C., & Lambert, D. L. 2008, *ApJ*, 680, 764

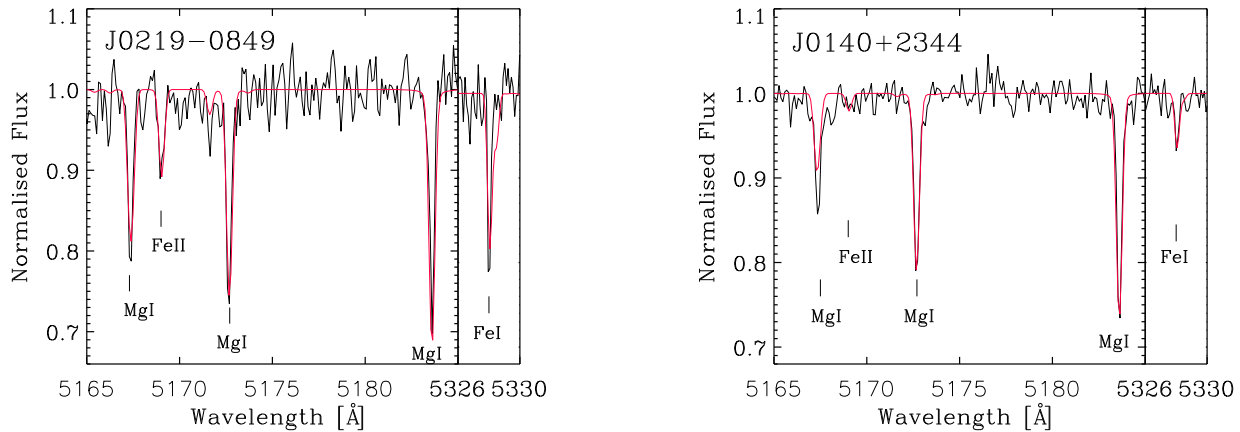


**Fig. 9.** Observed HRS spectra (black line) and best-fit synthetic spectra (red lines) of the Mg Ib triplet region in the stars J0219-0849 (left panel) and J0140+2344 (right panel).

- Kurucz, R. L. 2005, *Memorie della Societa Astronomica Italiana Supplementi*, 8, 14
- Lambert, D. L. & Sawyer, S. R. 1984, *ApJ*, 283, 192
- Lee, Y. S., Beers, T. C., Sivarani, T., et al. 2008a, *AJ*, 136, 2022
- Lee, Y. S., Beers, T. C., Sivarani, T., et al. 2008b, *AJ*, 136, 2050
- Maeder, A., Meynet, G., & Chiappini, C. 2015, *A&A*, 576, A56
- Masseron, T., Johnson, J. A., Plez, B., et al. 2010, *A&A*, 509, A93
- Mészáros, S., Allende Prieto, C., Edvardsson, B., et al. 2012, *AJ*, 144, 120
- Norris, J. E., Bessell, M. S., Yong, D., et al. 2013, *ApJ*, 762, 25
- Placco, V. M., Frebel, A., Lee, Y. S., et al. 2015, *ApJ*, 809, 136
- Ramsay, L. W., Adams, M. T., Barnes, T. G., et al. 1998, in *Proc. SPIE*, Vol. 3352, *Advanced Technology Optical/IR Telescopes VI*, ed. L. M. Stepp, 34–42
- Reddy, B. E., Lambert, D. L., & Allende Prieto, C. 2006, *MNRAS*, 367, 1329
- Sbordone, L. 2005, *Memorie della Societa Astronomica Italiana Supplementi*, 8, 61
- Sbordone, L., Bonifacio, P., Caffau, E., et al. 2010, *A&A*, 522, A26
- Shetrone, M., Cornell, M. E., Fowler, J. R., et al. 2007, *PASP*, 119, 556
- Sivarani, T., Beers, T. C., Bonifacio, P., et al. 2006, *A&A*, 459, 125
- Smee, S. A., Gunn, J. E., Uomoto, A., et al. 2013, *AJ*, 146, 32
- Snedden, C. A. 1973, PhD thesis, THE UNIVERSITY OF TEXAS AT AUSTIN.
- Spite, M., Caffau, E., Bonifacio, P., et al. 2013, *A&A*, 552, A107
- Spite, M., Cayrel, R., Plez, B., et al. 2005, *A&A*, 430, 655
- Starkenburg, E., Shetrone, M. D., McConnachie, A. W., & Venn, K. A. 2014, *MNRAS*, 441, 1217
- Tody, D. 1993, in *Astronomical Society of the Pacific Conference Series*, Vol. 52, *Astronomical Data Analysis Software and Systems II*, ed. R. J. Hanisch, R. J. V. Brissenden, & J. Barnes, 173
- Tominaga, N., Iwamoto, N., & Nomoto, K. 2014, *ApJ*, 785, 98
- Tull, R. G., MacQueen, P. J., Good, J., Epps, H. W., & HET HRS Team. 1998, in *Bulletin of the American Astronomical Society*, Vol. 30, *American Astronomical Society Meeting Abstracts*, 1263
- Yanny, B., Rockosi, C., Newberg, H. J., et al. 2009, *AJ*, 137, 4377
- Yong, D., Carney, B. W., & Friel, E. D. 2012, *AJ*, 144, 95
- Yong, D., Norris, J. E., Bessell, M. S., et al. 2013, *ApJ*, 762, 26

## Appendix A: Tables

We present a table with observing runs details.

**Table A.1.** The ISIS/WHT and HRS/HET Observing log.

Star	$g$ mag	$N_{\text{exp}} \times t_{\text{exp}}$	observing run	literature	S/N at 4500 Å
<b>ISIS/WHT</b>					
SDSS J010505+461521	19.3	13x1200 s	I		38
SDSS J014036+234458	15.8	2x1200 s	I	1,2	90
SDSS J021958-084955	16.4	4x1200 s	I		80
SDSS J040114-051259	18.6	5x1800 s	IV	2	37
SDSS J044655+113741	18.6	4x1200 s	I		22
SDSS J063055+255243	18.1	4x1800 s	IV		40
SDSS J075818+653906	17.7	6x1800 s	IV		60
SDSS J101600+172901	16.6	1x1200 s	II		33
SDSS J120441+120111	16.4	2x1800 s	II	4	50
SDSS J123055+000547	14.8	1x600 s	II		58
SDSS J132250+012343	16.3	1x2400 s	III	4	60
SDSS J134338+484426	12.5	2x1800 s	III		487
SDSS J164234+443004	17.8	5x1800 s	IV		39
SDSS J165618+342523	15.7	2x1800 s	II		70
SDSS J183455+421328	19.1	4x1800 s	I		24
SDSS J214633-003910	18.1	5x1200 s	I	2	40
SDSS J220646-092545	15.4	2x1200 s	I		110
2MASS J204523-284235	14.0	1x1200 s	II	1	118
<b>HRS/HET</b>					
SDSS J014036+234458	15.8	4x1500 s	11/12 dec 2012	1,2	80 at 5500 Å
SDSS J021958-084955	16.4	8x3400 s	6 dec 2012 /13 feb 2013		52 at 5500 Å

<sup>1</sup>Yong et al. (2013); <sup>2</sup>Caffau et al. (2013); <sup>3</sup>Caffau et al. (2011) <sup>4</sup>Placco et al. (2015); <sup>5</sup>Frebel et al. (2005); <sup>6</sup>Frebel et al. (2006)